

# ARE THERE MAGNETARS IN HIGH MASS X-RAY BINARIES? THE CASE OF SUPERGIANT FAST X-RAY TRANSIENTS

E. BOZZO<sup>1,2</sup>, M. FALANGA<sup>3</sup>, L. STELLA<sup>1</sup>

*Draft version November 13, 2018*

## ABSTRACT

In this paper we survey the theory of wind accretion in high mass X-ray binaries hosting a magnetic neutron star and a supergiant companion. We concentrate on the different types of interaction between the inflowing wind matter and the neutron star magnetosphere that are relevant when accretion of matter onto the neutron star surface is largely inhibited; these include the inhibition through the centrifugal and magnetic barriers. Expanding on earlier work, we calculate the expected luminosity for each regime and derive the conditions under which transition from one regime to another can take place. We show that very large luminosity swings ( $\sim 10^4$  or more on time scales as short as hours) can result from transitions across different regimes. The activity displayed by supergiant fast X-ray transients, a recently discovered class of high mass X-ray binaries in our galaxy, has often been interpreted in terms of direct accretion onto a neutron star immersed in an extremely clumpy stellar wind. We show here that the transitions across the magnetic and/or centrifugal barriers can explain the variability properties of these sources as a results of relatively modest variations in the stellar wind velocity and/or density. According to this interpretation we expect that supergiant fast X-ray transients which display very large luminosity swings and host a slowly spinning neutron star are characterized by magnetar-like fields, irrespective of whether the magnetic or the centrifugal barrier applies. Supergiant fast X-ray transients might thus provide a new opportunity to detect and study magnetars in binary systems.

*Subject headings:* accretion, accretion disks — stars: neutron — supergiant — X-rays: binaries — X-rays: stars

## 1. INTRODUCTION

High mass X-ray binaries (HMXBs) consist of a collapsed object, usually a magnetic neutron star (NS), that accretes matter from an OB companion star. Mass transfer takes place because of the intense stellar wind from the OB star, part of which is captured by the collapsed object (e.g. Verbunt & van den Heuvel 1995). Only in some short orbital period systems, the early type star, often a supergiant, fills its Roche lobe and leads to mass transfer through Roche lobe overflow (Tauris & van den Heuvel 2006). Persistent HMXBs accrete all the time and in most cases display X-ray luminosities in the  $10^{35}$ - $10^{38}$  erg s<sup>-1</sup> range. Many HMXBs are transient systems that remain at low X-ray luminosity levels ( $10^{32}$ - $10^{33}$  erg s<sup>-1</sup>) most of the time and undergo outbursts lasting from weeks to months. During these outbursts they display nearly identical properties to those of persistent HMXBs. Transient systems usually comprise a Be star donor and relatively long, moderately eccentric orbits, such that the star sits deep in its Roche lobe and stellar wind capture is the only mechanism through which mass transfer takes place. The occurrence of the outbursts is likely associated to variations in the stellar wind of the Be star, such as shell ejection episodes, or build up of matter around the resonant orbits in the slow equatorial wind component (van den Heuvel & Rappaport 2005). However, there are characteristics of the outbursts that are difficult to interpret if accretion onto the neutron star surface takes place unimpeded also in quiescence; these are (a) the large outburst to quiescence X-ray luminosity swing (factor of  $\sim 10^3$  or larger) and (b) the presence in a given source of low-luminosity (Type I) outbursts recurring close to periastron and, at different times, of high-luminosity (Type II) outbursts that last for several orbital cycles and display little (if any) X-ray flux variations associated to the orbital phase. These characteristics of Be transients can be explained if the accretion rate (and thus X-ray luminosity) variations that are produced by the stellar wind alone, could be amplified by some “gating” mechanism. Since most Be star HMXB transients contain relatively fast spinning X-ray pulsars, such mechanism has been identified with the centrifugal barrier that results from the rotation of the neutron star magnetosphere (Stella et al. 1986).

About 10 transient systems have been recently discovered, which display sporadic outbursts lasting from minutes to hours (i.e. much shorter than Be star transients’) and reach peak luminosities of  $\sim 10^{36}$ - $10^{37}$  erg s<sup>-1</sup>. These systems spend long time intervals in quiescence, with X-ray luminosities down to  $\sim 10^{-5}$  times lower than those in outburst; in spite of their association with OB supergiant companions, their behaviour is thus at variance with other persistent and transient HMXBs. They define a new class of HMXBs, collectively termed supergiant fast X-ray transients, SFXTs. An overview of the properties of SFXTs is given in § 2.

If accretion onto the collapsed object of SFXTs takes place both in quiescence and outburst, then the corresponding

<sup>1</sup> INAF - Osservatorio Astronomico di Roma, Via Frascati 33, 00044 Rome, Italy

<sup>2</sup> Dipartimento di Fisica - Università di Roma “Tor Vergata”, via della Ricerca Scientifica 1, 00133 Rome, Italy

<sup>3</sup> CEA Saclay, DSM/DAPNIA/Service d’Astrophysique (CNRS FRE 2591), F-91191, Gif sur Yvette, France

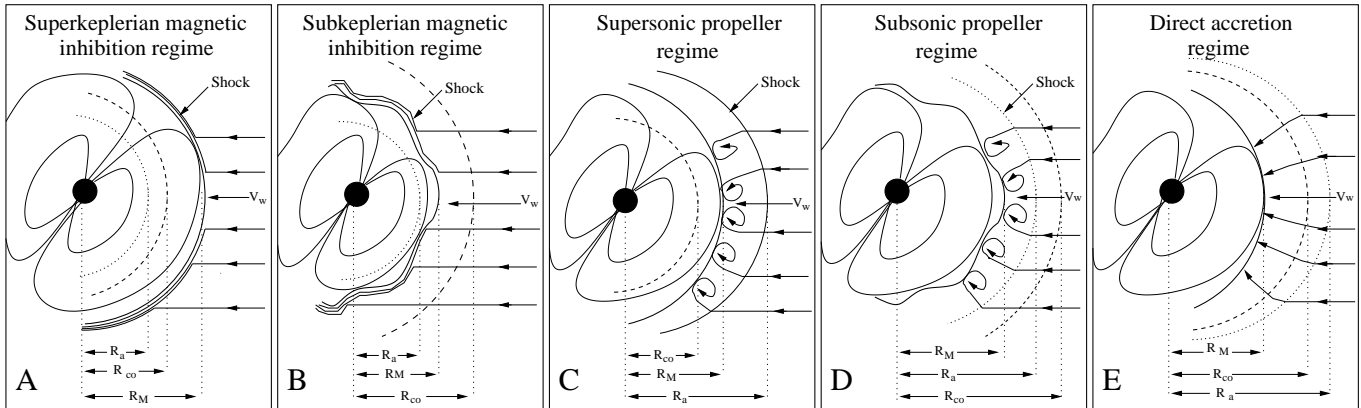


FIG. 1.— Schematic view of a magnetized NS interacting with the inflowing matter from its supergiant companion. All the regimes of § 3 are shown, together with the relative position of the magnetospheric radius (solid line), the corotation radius (dashed line), and the accretion radius (dotted line). A wavy solid line is used when the magnetospheric boundary at  $R_M$  is Kelvin-Helmholtz unstable. In the supersonic and subsonic propeller regime convective motions at the base of the atmosphere are represented with small eddies.

X-ray luminosity swing, typically a factor of  $\sim 10^4$ - $10^5$ , would require wind inhomogeneities with a very large density and/or velocity contrast (according to the standard wind accretion, the mass capture rate onto the NS scales like  $\dot{M}_w v_w^{-4}$ , with  $\dot{M}_w$ , the mass loss rate and  $v_w^{-4}$ , the wind velocity of the supergiant star, Davidson & Ostriker 1979). Several authors (In't Zand 2005; Leyder et al. 2007; Walter & Zurita Heras 2007) suggested the presence of dense clumps in the wind of the OB companions in order to attain the luminosity variations of SFXTs. While some observations provide evidence for a clumpy wind, the characteristics of such inhomogeneities are still poorly known. Numerical simulations suggest that clumps may originate from small scale perturbations in the radiation-driven wind (Dessart & Owocki 2003; Prinja et al. 2005). Models involving accretion of clumps are still being actively pursued (Negueruela et al. 2008; Walter & Zurita Heras 2007). The requirement on the density and/or velocity contrasts in the wind can be eased if there is a barrier that remains closed during quiescence, halting most of the accretion flow, and opens up in outbursts, leading to direct accretion (this is similar to the case of Be star transients). This paper develops and discusses gated accretion models for SFXTs.

In § 3 after reviewing the theory of wind accretion in HMXBs, we describe the different regimes of a rotating magnetic neutron star immersed the stellar wind from its companion. In § 4 we discuss the conditions under which transitions across regimes can take place in response to variations in the wind parameters. As compared to previous works addressing gating mechanisms in transient accreting magnetic neutron stars (notably Stella et al. 1986), we present here a more comprehensive treatment of the different physical processes that have been discussed in this context.

In § 5, we present an application to the different states of two SFXTs and discuss in turn the possibility that the outbursts are driven by a centrifugal or a magnetic barrier. The latter mechanism involves a magnetosphere extending beyond the accretion radius (Bondi 1952), which prevents most of the inflowing matter from accreting; it is discussed here for the first time in relation to the activity of transient binary sources. Unless the stellar wind were extremely clumpy (as envisaged in other SFXT models), the onset of a barrier inhibiting direct accretion would be required to explain the activity of SFXTs. In this case we conclude that if SFXTs host slowly rotating neutron stars (spin periods of several hundreds to thousands seconds), then they must possess magnetar-like fields ( $\sim 10^{14}$ - $10^{15}$  G), independent of whether the centrifugal or magnetic barrier operates. We summarize our discussion and conclusions in § 6 and § 7.

## 2. THE OBSERVED PROPERTIES OF SFXTS

SFXTs are observed to exhibit sporadic outbursts, lasting from minutes to hours, with peak X-ray luminosities between  $\sim 10^{36}$  and  $10^{37}$  erg s $^{-1}$  (see e.g., González-Riestra et al. 2004; Sidoli et al. 2005; Grebenev & Sunyaev 2005; Lutovinov et al. 2005; Sguera et al. 2005; Masetti et al. 2006; Sguera et al. 2006; Götz et al. 2007; Sguera et al. 2007). No firm orbital period measurement has been obtained yet<sup>4</sup>. A recent list of confirmed ( $\sim 5$ ) and candidate ( $\sim 6$ ) SFXTs is given by Walter & Zurita Heras (2007).

Between outbursts, SFXTs remain in quiescence with luminosities in the range  $\sim 10^{31}$ - $10^{33}$  erg s $^{-1}$  (González-Riestra et al. 2004; In't Zand 2005; Smith et al. 2006; Kennea & Campana 2006). In some cases, very high peak-to-quiescence X-ray luminosity swings (factor of  $\sim 10^4$ - $10^5$ ) were seen on timescales comparable to the outburst duration. Some SFXTs showed also flare-like activity at intermediate luminosity levels (e.g., González-Riestra et al. 2004). In the case of IGR J17544-2619, two states of intermediate luminosity were observed: one before the onset of the outburst and the other immediately after, with X-ray luminosities  $\sim 3$  and  $\sim 1$  decades below the value reached at the peak of the outburst, respectively (In't Zand 2005).

The sporadic character of SFXT outbursts, as observed with *INTEGRAL*, suggested that the duty cycle of these

<sup>4</sup> Only IGR J11215-5952 and AX J1749.1-2733 showed recurrent flaring activity, with periodicity of  $\sim 165$  d and  $\sim 185$  d, respectively. These are interpreted as outbursts from two systems with unusually long orbital periods ( $\gtrsim 100$  d, Grebenev & Sunyaev 2005; Sidoli et al. 2007; Zurita Heras et al. 2007). Thus Walter & Zurita Heras (2007) excluded these sources from their SFXT list.

sources (the fraction of time spent in a high luminosity state) is small ( $\sim 0.02$ - $0.002$ , Walter & Zurita Heras 2007). However, recent observations carried out with the very sensitive X-ray telescopes on board *XMM-Newton* and *Chandra* revealed that some SFXTs display flares around a luminosity of  $\gtrsim 10^{34}$ - $10^{35}$  erg s $^{-1}$  (i.e. well below the *INTEGRAL* limiting sensitivity) for a large fraction of the time (González-Riestra et al. 2004; In't Zand 2005; Tomsick et al. 2006). Therefore, the indication is that the active phase of SFXT sources (as opposed to true quiescence) lasts longer than previously thought, and the duty cycles are of order  $\sim 0.1$  or higher.

Optical identifications of SFXTs show that these sources are associated to OB supergiant companion stars (see e.g., Walter & Zurita Heras 2007, and reference therein). The SFXT OB companions have typically mass of  $M_* \sim 30 M_\odot$ , luminosity of  $\log(L_*/L_\odot) \sim 5$ - $6$ , mass loss rate of  $\dot{M}_w = 10^{-7}$ - $10^{-5} M_\odot \text{ yr}^{-1}$ , and wind velocity of  $1000$ - $2000 \text{ km s}^{-1}$ . Note, that isolated OB stars with  $\log(L_*/L_\odot) \sim 5$ - $6$  are persistent soft X-ray sources with luminosity around  $\sim 10^{32}$  erg s $^{-1}$  (Cassinelli et al. 1981; Berghoefter et al. 2001).

It is widely believed that SFXTs contain sporadically accreting neutron stars. Only little is known about their spin period. A coherent periodicity was detected at  $4.7 \text{ s}$  and  $228 \text{ s}$  in AX J1841.0-0536 and IGR J16465-4507, respectively (Bamba et al. 2001; Lutovinov et al. 2005). However, IGR J16465-4507 showed only a factor of  $\sim 100$  luminosity swing between quiescence and outburst, so it is unclear whether the source should be considered a transient (in fact it is classified as an “intermediate system”, Walter & Zurita Heras 2007). The nature of the companion star in AX J1841.0-0536 is still debated (Halpern et al. 2004; Nespoli et al. 2007). Therefore, these two sources might not belong to the SFXT class. On the contrary, in the prototypical SFXTs XTE J1739-302 (Sguera et al. 2006) and IGR J16479-4514 (Walter et al. 2006) some evidence has been reported for periodicities in the  $\sim 1000$ - $2000 \text{ s}$  range. We assume in the following that SFXTs host a rotating magnetic neutron star.

### 3. STELLAR WIND ACCRETION

We investigate here the conditions under which a magnetized neutron star can accrete matter from the wind of a massive companion. In the theory of wind accretion in HMXBs, the following radii are defined (see e.g., Illarionov & Sunyaev 1975; Stella et al. 1986):

- The accretion radius,  $R_a$  is the distance at which the inflowing matter is gravitationally focused toward the NS (Bondi 1952). It is usually expressed as

$$R_a = 2GM_{\text{NS}}/v_w^2 = 3.7 \times 10^{10} v_8^{-2} \text{ cm}, \quad (1)$$

where  $v_8$  is the wind velocity in units of  $1000 \text{ km s}^{-1}$  and we assumed that the orbital velocity of the star is negligible (Frank et al. 2002). Throughout the paper we fix the NS radius and mass at  $R_{\text{NS}} = 10^6 \text{ cm}$  and  $M_{\text{NS}} = 1.4 M_\odot$ , respectively. The fraction  $\dot{M}_{\text{capt}}/\dot{M}_w$  of the stellar wind mass loss rate ( $\dot{M}_w$ ) captured by the NS depends on  $R_a$  through (Frank et al. 2002)

$$\dot{M}_{\text{capt}}/\dot{M}_w \simeq R_a^2/(4a^2) = 2 \times 10^{-5} v_8^{-4} a_{10\text{d}}^{-2}. \quad (2)$$

Here  $a = 4.2 \times 10^{12} a_{10\text{d}} \text{ cm}$  is the orbital separation,  $a_{10\text{d}} = P_{10\text{d}}^{2/3} M_{30}^{1/3}$ ,  $P_{10\text{d}}$  is the binary orbital period in units of 10 days, and  $M_{30}$  is the total mass in units of  $30 M_\odot$  (we assumed circular orbits).

- The magnetospheric radius,  $R_M$ , at which the pressure of the NS magnetic field ( $\mu^2/(8\pi R_{\text{NS}}^6)$ , with  $\mu$  the NS magnetic moment) balances the ram pressure of the inflowing matter ( $\rho_w v_w^2$ ). In the case in which  $R_M > R_a$ , the magnetospheric radius is given by (Davies & Pringle 1981)

$$R_M = 3.3 \times 10^{10} \dot{M}_{-6}^{-1/6} v_8^{-1/6} a_{10\text{d}}^{1/3} \mu_{33}^{1/3} \text{ cm}. \quad (3)$$

Here we assumed a non magnetized spherically symmetric wind (Elsner & Lamb 1977), with density<sup>5</sup>  $\rho_w(R_M) \sim \dot{M}_w/(4\pi a^2 v_w)$ , a dipolar NS magnetic field with  $\mu_{33} = \mu/10^{33} \text{ G cm}^3$ , and  $\dot{M}_{-6} = \dot{M}_w/10^{-6} M_\odot \text{ yr}^{-1}$ . In the following sections we discuss the range of applicability of Eq. 3, and the regimes in which a different prescription for  $R_M$  should be used.

- The corotation radius,  $R_{\text{co}}$ , at which the NS angular velocity equals the Keplerian angular velocity, i.e.

$$R_{\text{co}} = 1.7 \times 10^{10} P_{s3}^{2/3} \text{ cm}. \quad (4)$$

Here  $P_{s3}$  is the NS spin period in units of  $10^3 \text{ s}$ .

Changes in the relative position of these radii result into transitions across different regimes for the NS (Illarionov & Sunyaev 1975; Stella et al. 1986). Below we discuss these regimes singularly, and provide a schematic representation of each regime in Fig. 1. Being determined primarily by the spin of the neutron star, the corotation radius can change only over evolutionary timescales. Illarionov & Sunyaev (1975) summarises the different regimes experienced by a spinning down NS since its birth, from the initial radio pulsar (i.e. rotation powered) stage, to the regime in which mass accretion onto the neutron star surface can take place. On the other hand the accretion radius and magnetospheric radius depend on the wind parameters (see Eqs. 1 and 3), which can vary on a wide range of

<sup>5</sup> We approximated  $a/R_M \simeq a$ , which is satisfied for a very wide range of parameters.

timescales (from hours to months). Therefore, variations in the wind parameters can cause the neutron star to undergo transitions across different regimes on comparably short timescales, thus opening the possibility to explain the properties of some classes of highly variable X-ray sources through them. In particular, the transition from the accretion regime to the propeller regime (and vice versa), across the so-called ‘‘centrifugal barrier’’, was identified as a likely mechanism responsible for the pronounced activity of Be X-ray pulsar transient systems (Stella et al. 1986). Below we summarise the different regimes of a magnetic rotating neutron star, subject to a varying stellar wind, with special attention to the condition under which a ‘‘magnetic’’ (as opposed to ‘‘centrifugal’’) barrier inhibits accretion onto the neutron star (Harding et al. 1992; Rutledge 2001; Mori & Ruderman 2003; Toropina et al. 2006, 2001). As it will be clear in the following, new motivation for investigating magnetic inhibition of accretion comes from the discovery of magnetars, neutrons stars with extremely high magnetic fields ( $\sim 10^{14}$ - $10^{15}$  G, Duncan & Thompson 1992).

### 3.1. Outside the accretion radius: the magnetic inhibition of accretion: $R_M > R_a$

We consider here the case in which the magnetospheric radius is larger than the accretion radius<sup>6</sup>. In systems with  $R_M > R_a$  the mass flow from the companion star interacts directly with the NS magnetosphere without significant gravitational focusing, forming a bow shock at  $R_M$  (Harding et al. 1992; Toropina et al. 2001). A region of shocked gas surrounds the NS magnetosphere with density  $\rho_{ps} \simeq 4\rho_w$  and velocity  $v_{ps} \simeq v_w/4$  (the subscript ‘‘ps’’ stands for post-shock). These are only rough estimates because the shock is very close to the magnetopause and it does not satisfy the standard Rankine-Hugoniot conditions (Toropina et al. 2001). At least in the front part of the shock, i.e. in the region around the stagnation point, the whole kinetic energy of the inflowing matter is converted into thermal energy, and the expected temperature of the heated gas is  $T \simeq m_p v_w^2 / (3k) \simeq 4 \times 10^7 v_8^2$  K. Thus, the power released in this region is of order

$$L_{\text{shock}} \simeq \frac{\pi}{2} R_M^2 \rho_w v_w^3 = 4.7 \times 10^{29} R_{M10}^2 v_8^2 a_{10d}^{-2} \dot{M}_{-6} \text{ erg s}^{-1} \quad (5)$$

( $R_{M10}$  is the magnetospheric radius in units of  $10^{10}$  cm), and is mainly radiated in the X-ray band (Toropina et al. 2006). Below we distinguish two different regimes of magnetic inhibition of accretion.

#### 3.1.1. The superKeplerian magnetic inhibition regime: $R_M > R_a, R_{co}$

In this ‘‘superKeplerian’’ magnetic inhibition regime the magnetospheric radius is larger than both the accretion and corotation radii ( $R_M > R_a, R_{co}$ ). Matter that is shocked and halted close to  $R_M$  cannot proceed further inward, due to the rotational drag of the NS magnetosphere which is locally superKeplerian. Since magnetospheric rotation is also supersonic<sup>7</sup>, the interaction between the NS magnetic field and matter at  $R_M$  results in rotational energy dissipation and thus, NS spin down. In order to derive an upper limit on the contribution of this dissipation to the overall luminosity, we assume that the above interaction is anelastic (e.g., Perna et al. 2006), i.e. that matter at  $R_M$  is forced to corotate. This process releases energy at a rate

$$L_{sd} \simeq \pi R_M^2 \rho_w v_w (R_M \Omega)^2 \simeq 3.7 \times 10^{29} R_{M10}^4 \dot{M}_{-6} a_{10d}^{-2} P_{s3}^{-2} \text{ erg s}^{-1}, \quad (6)$$

which adds to the shock luminosity (Eq. 5).

#### 3.1.2. The subKeplerian magnetic inhibition regime: $R_a < R_M < R_{co}$

If  $R_a < R_M < R_{co}$  the magnetospheric drag is subKeplerian and matter can penetrate the NS magnetosphere. In this ‘‘subKeplerian’’ magnetic inhibition regime, the boundary between the inflowing matter and the magnetosphere is subject to the Kelvin-Helmholtz instability (KHI, Harding et al. 1992). The mass inflow rate across  $R_M$  resulting from the KHI is approximately (Burnard et al. 1983)

$$\dot{M}_{KH} \simeq 2\pi R_M^2 \rho_{ps} v_{conv} = 2\pi R_M^2 \rho_{ps} v_{sh} \eta_{KH} (\rho_i / \rho_e)^{1/2} (1 + \rho_i / \rho_e)^{-1}, \quad (7)$$

where  $\eta_{KH} \sim 0.1$  is an efficiency factor,  $v_{sh}$  is the shear velocity,  $\rho_i$  and  $\rho_e$  the density inside and outside the magnetospheric boundary at  $R_M$ , respectively. Close to the stagnation point, virtually all the kinetic energy of the wind matter is converted into thermal energy (see also § 3.1.1), and the shear velocity is thus dominated by the magnetosphere’s rotation, such that  $v_{sh} = v_{rot} = 2\pi P_s^{-1} R_M$ . Away from this region, the tangential component of the wind velocity with respect to the NS magnetic field lines increases up to  $v_{ps}$  and, in general, the shear velocity and rate at which plasma enters the magnetosphere due to the KHI, depends on both  $v_{ps}$  and  $v_{rot}$ . For the aims of this paper, we adopt  $v_{sh} = \max(v_{ps}, v_{rot})$ , and use mass conservation across the KHI unstable layer to estimate the density ratio at  $R_M$  (Burnard et al. 1983). If matter crossing the unstable layer of height  $h_t$  is rapidly brought into corotation with the NS magnetosphere and free-falls onto the NS, mass conservation implies

$$R_M^2 \rho_e v_{conv} \simeq R_M h_t \rho_i v_{ff}(R_M). \quad (8)$$

The height  $h_t$  of the unstable layer, where matter and magnetic field coexist, is mostly determined by the largest wavelength of the KHI unstable mode (Burnard et al. 1983). A detailed analysis of this instability is beyond the scope

<sup>6</sup> A similar case was considered also by Lipunov (1992), ‘‘the georotator regime’’, and by Toropina et al. (2001), ‘‘the magnetic plow regime’’.

<sup>7</sup> This can be easily seen by comparing  $v_w$  with  $\Omega R_M$ , for the value of the parameters used in this section.

of this paper. In Eq. 8 we use conservatively  $h_t \simeq R_M$ , and discuss in Appendix A the effect of smaller values of  $h_t$ . Therefore accretion of matter at a rate  $\dot{M}_{KH}$  onto the NS is expected to release a luminosity of

$$L_{KH} = 3.5 \times 10^{34} \eta_{KH} R_{M10}^2 a_{10d}^{-2} \dot{M}_{-6} (\rho_i/\rho_e)^{1/2} (1 + \rho_i/\rho_e)^{-1} \text{ erg s}^{-1}, \quad (9)$$

if  $v_{sh} = v_{ps}$ , or

$$L_{KH} = 8.8 \times 10^{34} \eta_{KH} P_{s3}^{-1} R_{M10}^3 a_{10d}^{-2} v_8^{-1} \dot{M}_{-6} (\rho_i/\rho_e)^{1/2} (1 + \rho_i/\rho_e)^{-1} \text{ erg s}^{-1}, \quad (10)$$

if  $v_{sh} = v_{rot}$ . The values of  $\rho_i/\rho_e$  that we use in Eqs. 9 and 10 are derived numerically from Eq. 8.

In the subKeplerian magnetic inhibition regime, plasma penetration inside the NS magnetosphere is sustained also by Bohm diffusion (Ikhsanov & Pustil'nik 1996). This diffusion, being dependent on the temperature of the plasma (rather than velocity), is highest in the region close to the stagnation point, where the shock slows down the inflowing plasma most efficiently (see also § 3.1.1). In accordance with Ikhsanov et al. (2001b), the maximum inflow rate allowed by Bohm diffusion is

$$\dot{M}_{diff} \simeq 2\pi R_M^2 \rho_{ps} V_m = 4.5 \times 10^9 \zeta^{1/2} \dot{M}_{-6} \mu_{33}^{-1/2} R_{M10}^{11/4} a_{10d}^{-2} \text{ g s}^{-1}, \quad (11)$$

where  $V_m = \sqrt{D_{eff}/t_{ff}}$  is the diffusion velocity,  $D_{eff} = (\zeta ck T_i(R_M))/(16eB(R_M))$  the diffusion coefficient,  $T_i(R_M) \simeq m_p v_w^2/(3k)$  the post-shock ion temperature,  $t_{ff} = \sqrt{R_M^3/(2GM)}$  the free-fall time,  $\zeta \simeq 0.1$  an efficiency factor and  $m_p$  the proton mass. In the above equation we also approximated the density outside  $R_M$ , around the stagnation point, with  $\rho_{ps}$  (though this might be underestimate by a factor of a few, see Toropina et al. 2001). Over the whole range of parameters relevant to this work, the diffusion-induced mass accretion rate is orders of magnitude smaller than that due to the KHI. Similarly, the contribution to the total luminosity resulting from the shock and anelastic drag at the magnetospheric boundary can be neglected in this regime.

### 3.2. Inside the accretion radius: $R_M < R_a$

#### 3.2.1. The supersonic propeller regime: $R_{co} < R_M < R_a$

Once  $R_M$  is inside the accretion radius, matter flowing from the companion star is shocked adiabatically at  $R_a$  and halted at the NS magnetosphere. In the region between  $R_a$  and  $R_M$  this matter redistributes itself into an approximately spherical configuration (resembling an ‘‘atmosphere’’), whose shape and properties are determined by the interaction between matter and NS magnetic field at  $R_M$ . This scenario was considered previously by Davies et al. (1979) and Davies & Pringle (1981), and we follow here their treatment. These authors demonstrated that hydrostatic equilibrium ensues when radiative losses inside  $R_a$  are negligible (we discuss this approximation in Appendix B and C) and the atmosphere is stationary on dynamical time-scales. Assuming a polytropic law of the form  $p \propto \rho^{1+1/n}$ , the pressure and density of this atmosphere are:

$$p(R) = \rho_{ps} v_{ps}^2 [1 + (1/(1+n))8R_a/R]^{n+1} \quad (12)$$

$$\rho(R) = \rho_{ps} [1 + (1/(1+n))8R_a/R]^n. \quad (13)$$

The value of the polytropic index  $n$  depends on the conditions at the inner boundary of the atmosphere, and in particular on the rate at which energy is deposited there.

When the rotational velocity of the NS magnetosphere at  $R_M$  is supersonic (see also § 3.1.1), the interaction with matter in the atmosphere leads to dissipation of some of the star’s rotational energy and thus spin-down. In the supersonic propeller regime, Davies & Pringle (1981) showed that turbulent motions are generated at  $R_M$  which convect this energy up through the atmosphere, until it is lost at its outer boundary. In this case  $n=1/2$ . Accordingly, taking into account the structure of the surrounding atmosphere, the magnetospheric radius is given by

$$R_M^{-6} (1 + 16R_a/(3R_M))^{-3/2} = \frac{1}{2} \dot{M}_w a^{-2} \mu^{-2} v_w. \quad (14)$$

This can be approximated by

$$R_M \simeq 2.3 \times 10^{10} a_{10d}^{4/9} \dot{M}_{-6}^{-2/9} v_8^{4/9} \mu_{33}^{4/9} \text{ cm}. \quad (15)$$

Matter that is shocked at  $\sim R_a$ , reaches the magnetospheric boundary at  $R_M$  where the interaction with the NS magnetic field draws energy from NS rotation (see also § 3.1.1). According to Davies & Pringle (1981), this contributes

$$L_{sd} = 2\pi R_M^2 \rho(R_M) c_s^3(R_M) \simeq 5.4 \times 10^{31} \dot{M}_{-6} a_{10d}^{-2} v_8^{-1} R_{M10}^{1/2} (1 + 16R_{a10}/(3R_{M10}))^{1/2} \text{ erg s}^{-1} \quad (16)$$

to the total luminosity. In the above equation  $R_{a10} = 10^{-10} R_a$  and  $c_s(R_M) = v_{ff}(R_M) = (2GM_{NS}/R_M)^{1/2}$  (Davies & Pringle 1981). In the supersonic propeller regime the energy released through the shock at  $R_a$ ,

$$L_{shock} = \frac{9}{32} \pi R_a^2 \rho_w v_w^3 \simeq 2.6 \times 10^{29} R_{a10}^2 v_8^2 a_{10d}^{-2} \dot{M}_{-6} \text{ erg s}^{-1}, \quad (17)$$

is negligible.

### 3.2.2. The subsonic propeller regime: $R_M < R_a$ , $R_{co}$ , $\dot{M}_w < \dot{M}_{lim}$

The break down of the supersonic propeller regime occurs when  $R_M < R_{co}$ , i.e., when the magnetosphere rotation is no longer supersonic with respect to the surrounding material. The structure of the atmosphere changes and the transition to the subsonic propeller regime takes place. Since the rotation of the magnetosphere is subsonic, the atmosphere is roughly adiabatic ( $n=3/2$ ), and the magnetospheric radius is given by (Davies & Pringle 1981):

$$R_M^{-6} (1 + 16R_a/(5R_M))^{-5/2} = \frac{1}{2} \dot{M}_w a^{-2} \mu^{-2} v_w. \quad (18)$$

This can be approximated by

$$R_M \simeq 2 \times 10^{10} a_{10d}^{4/7} \dot{M}_{-6}^{-2/7} v_8^{8/7} \mu_{33}^{4/7} \text{ cm}. \quad (19)$$

In the subsonic propeller regime, the centrifugal barrier does not operate because  $R_M < R_{co}$ , but the energy input at the base of the atmosphere (due to NS rotational energy dissipation) is still too high for matter to penetrate the magnetosphere at a rate  $\dot{M}_{capt}$  (Davies & Pringle 1981). Nevertheless a fraction of the matter inflow at  $R_a$  is expected to accrete onto the NS, due to the KHI and Bohm diffusion<sup>8</sup>.

Based on the discussion in § 3.1.2, we estimate the accretion luminosity of this matter by using Eqs. 7 and 11 (we approximate here the surface of interaction between matter and magnetic field with  $4\pi R_M^2$ ). This gives

$$L_{diff} \simeq GM_{NS} \dot{M}_{diff} / R_{NS} = 4.5 \times 10^{30} \dot{M}_{-6} a_{10d}^{-2} R_{M10}^{9/4} \mu_{33}^{-1/2} \zeta^{1/2} v_8^{-1} (1 + 16R_{a10}/(5R_{M10}))^{3/2} \text{ erg s}^{-1}, \quad (20)$$

and

$$\begin{aligned} L_{KH} &\simeq GM_{NS} \dot{M}_{KH} / R_{NS} = \\ &1.8 \times 10^{35} \eta_{KH} P_{s3}^{-1} R_{M10}^3 \dot{M}_{-6} a_{10d}^{-2} v_8^{-1} (1 + 16R_{a10}/(5R_{M10}))^{3/2} (\rho_i/\rho_e)^{1/2} (1 + \rho_i/\rho_e)^{-1} \text{ erg s}^{-1}, \end{aligned} \quad (21)$$

for the accretion luminosity arising from matter entering the magnetosphere through Bohm diffusion and KHI, respectively. For the range of parameters of interest here, Eqs. 5, 20, and 21 show that  $L_{KH}$  dominates. The rotational energy dissipation at  $R_M$  (see § 3.2.1) gives a small contribution with respect to Eq. 21 (Davies & Pringle 1981):

$$L_{sd} = 2\pi R_M^5 \rho (R_M) \Omega^3 = 2.2 \times 10^{30} P_{s3}^{-3} R_{M10}^5 \dot{M}_{-6} v_8^{-1} a_{10d}^{-2} (1 + 16R_{a10}/(5R_{M10}))^{3/2} \text{ erg s}^{-1}. \quad (22)$$

The subsonic propeller regime applies until the critical accretion rate

$$\dot{M}_{lim-6} = 2.8 \times 10^2 P_{s3}^{-3} a_{10d}^2 v_8 R_{M10}^{5/2} (1 + 16R_{a10}/(5R_{M10}))^{-3/2} \quad (23)$$

is reached, at which the gas radiative cooling (bremsstrahlung) completely damps convective motions inside the atmosphere (see Appendix C). If this cooling takes place, direct accretion at a rate  $\dot{M}_{capt}$  onto the NS surface is permitted.

### 3.2.3. The direct accretion regime: $R_M < R_a$ , $R_{co}$ , $\dot{M}_w > \dot{M}_{lim}$

If  $R_M < R_{co}$  and matter outside the magnetosphere cools efficiently, accretion onto the NS takes place at the same rate  $\dot{M}_{capt}$  (see Eq. 2) at which it flows towards the magnetosphere. The corresponding luminosity is

$$L_{acc} = GM_{NS} \dot{M}_{capt} / R_{NS} = 2 \times 10^{35} \dot{M}_{-6} a_{10d}^{-2} v_8^{-4} \text{ erg s}^{-1} \simeq 2 \times 10^{35} \dot{M}_{15} \text{ erg s}^{-1}, \quad (24)$$

where  $\dot{M}_{15} = \dot{M}_{capt} / 10^{15} \text{ g s}^{-1}$ . This is the standard accretion regime; the system achieves the highest mass to luminosity conversion efficiency.

## 4. TRANSITIONS AND PATHS ACROSS DIFFERENT REGIMES

We explore here the conditions under which transitions across different regimes take place. As emphasised in § 3, these transitions occur when the relative positions of  $R_M$ ,  $R_a$ , and  $R_{co}$  change; we concentrate here on transitions that occur in response to variations in the stellar wind parameters. In the following, since  $R_M$  depends only weakly on the orbital period and the total mass of the system, we fix  $a_{10d}=1$  (we explain this choice in § 5), and investigate variations in the other four parameters:  $\mu_{33}$ ,  $P_{s3}$ ,  $v_8$ , and  $\dot{M}_{-6}$ .

The equations that define the conditions for transitions between different regimes are<sup>9</sup>

$$R_M > R_a \Rightarrow \dot{M}_{-6} \lesssim 0.45 \mu_{33}^2 v_8^{11} a_{10d}^2 \quad (25)$$

(or equivalently  $\dot{M}_{15} \lesssim 0.6 \mu_{33}^2 v_8^7$ , see Eqs. 1, 3 and 2), for the magnetic barrier;

$$R_M > R_{co} \Rightarrow P_{s3} \lesssim 2.6 \dot{M}_{-6}^{-1/4} v_8^{-1/4} a_{10d}^{1/2} \mu_{33}^{1/2} \simeq 2.8 \dot{M}_{15}^{-1/4} v_8^{-5/4} \mu_{33}^{1/2} \quad (26)$$

<sup>8</sup> To our knowledge this is the first application of the KHI to the subsonic propeller regime.

<sup>9</sup> Here we used Eqs. 15 and 19 for the magnetospheric radius in the supersonic and subsonic propeller regime, respectively.

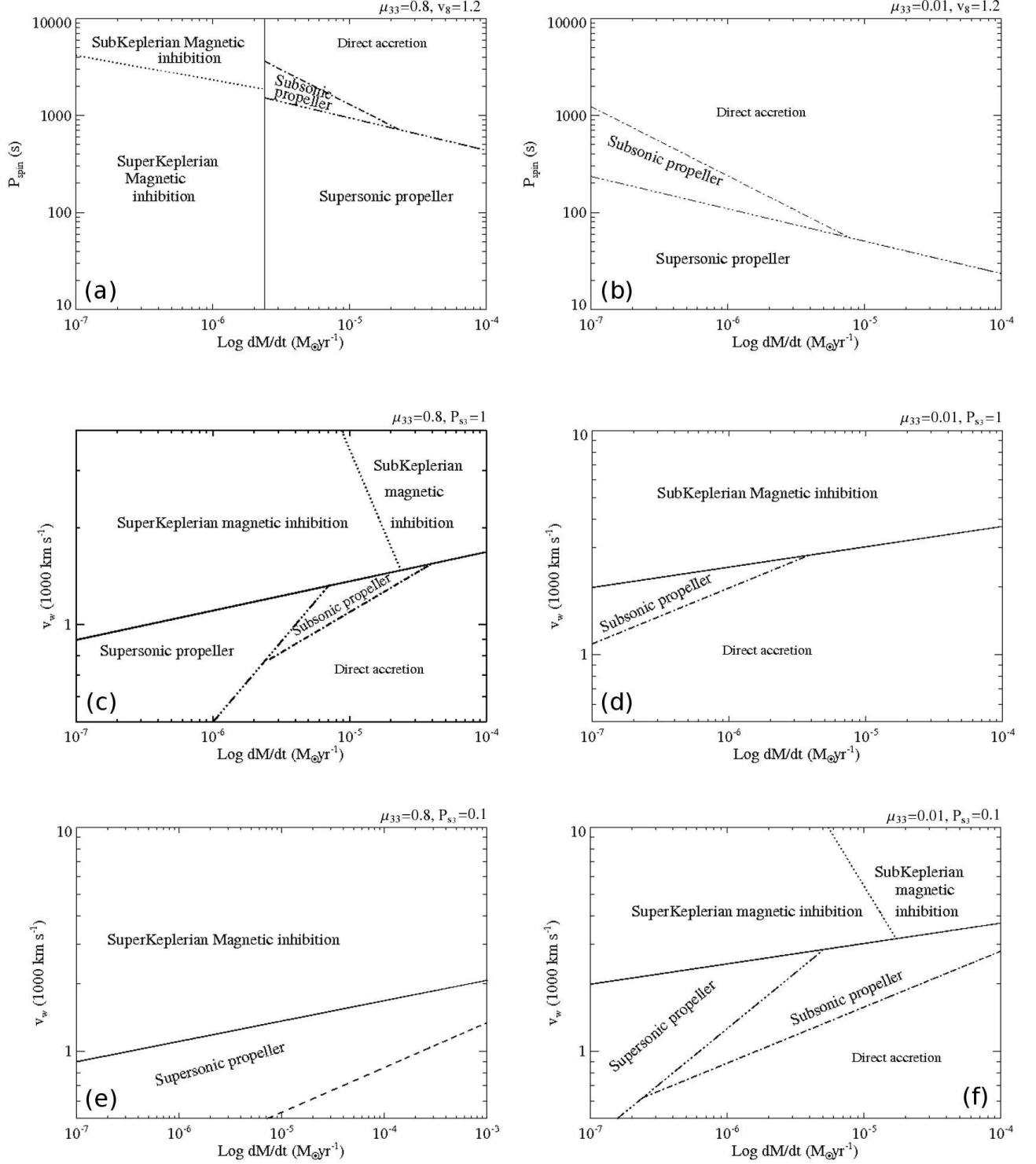


FIG. 2.— Transitions between regimes described in § 3 for selected values of the parameters  $\mu_{33}$ ,  $P_{s3}$ , and  $v_8$  (in each panel these parameters are indicated in the top right corner). In all cases we fixed  $a_{10d}=1$  (see § 4). In panels (a) and (b) we fixed  $\mu_{33}$  and  $v_8$  and investigated the different regimes in the  $P_{s3}-\dot{M}_6$  plane. In panels (c), (d), (e), and (f), instead, fixed parameters are  $P_{s3}$  and  $\mu_{33}$ , and the relevant regimes are shown in the  $v_8-\dot{M}_6$  plane. In all cases Eqs. 25, 26, 27, 28, and B2 (see Appendix B) are represented with a solid line, a dotted line, a dot-dot-dot dashed line, a dot-dashed line, and a dashed line, respectively. Note that the line from Eq. B2 is present only in panel (e), i.e our treatment of the the supersonic propeller is self-consistent everywhere except for a small region away from the range of interest for SFXT sources (see also § 5).

(see Eq. 3) if  $R_M > R_a$ , or

$$R_M > R_{co} \Rightarrow P_{s3} \lesssim 1.8 a_{10d}^{2/3} \dot{M}_{-6}^{-1/3} v_8^{2/3} \mu_{33}^{2/3} \simeq 2 \dot{M}_{15}^{-1/3} v_8^{-2/3} \mu_{33}^{2/3} \quad (27)$$

(see Eq. 15) if  $R_M < R_a$ , for the centrifugal barrier.

The equation that defines the transition from the subsonic propeller to the direct accretion regime is

$$P_{s3} \gtrsim 4.5 \dot{M}_{-6}^{-15/21} a_{10d}^{30/21} v_8^{60/21} \mu_{33}^{16/21} \simeq 5.5 \dot{M}_{15}^{-15/21} \mu_{33}^{16/21}. \quad (28)$$

In Fig. 2 the above equations are represented as lines separating different regimes. In panels (a) and (b) we fixed  $\mu_{33}$  and  $v_8$  and investigated the different regimes in the  $P_{s3}-\dot{M}_{-6}$  plane. In panels (c), (d), (e) and (f), instead,  $P_{s3}$  and  $\mu_{33}$  were fixed and the relevant regimes shown in the  $v_8-\dot{M}_{-6}$  plane. Below we summarise the different regimes that a system attains in response to variations of  $\dot{M}_w$ , in the different panels.

Panel (a) shows that, for a wind velocity of  $v_8=1.2$ , a strongly magnetized NS ( $\mu_{33}=0.8$ ) can undergo a transition between the superKeplerian and subKeplerian magnetic inhibition regimes in response to changes in the mass loss rate only for typical spin periods  $\gtrsim 2000$  s. When the mass loss rate reaches  $\dot{M}_{-6} \sim 2.4$ , the direct accretion or subsonic propeller regime sets in, depending on whether the spin period is longer or shorter than  $\sim 3700$  s. For spin periods  $\lesssim 420$  s the direct accretion regime is not attained for the interval of mass loss rates considered in Fig. 2 and only transitions between the superKeplerian magnetic inhibition and supersonic propeller regime are expected.

For lower magnetic fields ( $\mu_{33}=0.01$ ), panel (b) shows that only the supersonic propeller, subsonic propeller, and direct accretion regime can be attained. For spin periods in the range  $\sim 60$ -230 s transitions can occur between all these three regimes, whereas systems with spin periods longer than  $\sim 1300$  s and shorter than  $\sim 20$  s are expected to be in the direct accretion and the supersonic propeller regime, respectively. For  $\mu_{33}=0.01$  transitions to the superKeplerian and subKeplerian magnetic inhibition regimes cannot take place because the magnetospheric radius is too small to exceed the accretion radius.

In panel (c) ( $\mu_{33}=0.8$  and  $P_{s3}=1$ ), transitions can occur virtually between all the regimes described in § 3. In particular, for  $v_8$  in the range 0.9-1.5 transitions are expected to take place between the superKeplerian magnetic inhibition, the supersonic and subsonic propeller, and the direct accretion regime, as the mass loss rate increases from  $\dot{M}_{-6} \sim 0.1$  to  $\dot{M}_{-6} \sim 100$ . For velocities  $v_8 < 0.9$  transitions can occur only between the supersonic propeller, the subsonic propeller and the direct accretion regime, whereas transitions to the superKeplerian and subKeplerian magnetic inhibition regimes are impeded by the fact that the accretion radius cannot be overtaken by  $R_M$ . On the contrary, for  $v_8 > 1.5$ , the magnetospheric radius is located beyond the accretion radius for any considered value of the mass loss rate, and thus transitions can take place only between the superKeplerian and subKeplerian magnetic inhibition regimes. Similar considerations apply to panels (d), (e), and (f).

For a system with  $\mu_{33}=0.01$  and  $P_{s3}=1$  (panel (d)), the superKeplerian magnetic inhibition regime never occurs, because the magnetic field is too low and  $R_M < R_{co}$  for any  $0.1 < \dot{M}_{-6} < 100$ . Instead, the subKeplerian magnetic inhibition regime can be attained for high wind velocities ( $v_8=2$ ), because  $R_a \propto v_w^{-2}$ .

In panel (e), for  $\mu_{33}=0.8$  and  $P_{s3}=0.1$ , the magnetospheric radius is larger than the corotation radius for the entire range spanned by  $\dot{M}_{-6}$ . Thus accretion onto the NS does not take place (note that in the region below the dashed line accretion can occur even if  $R_M \gtrsim R_{co}$ , Davies & Pringle 1981)<sup>10</sup>.

Finally, in panel (f) we show the transitions for a system with  $\mu_{33}=0.01$  and  $P_{s3}=0.1$  s. In this case all the regimes described in § 3 are present in the figure, similar to the case of panel (c). However, the region corresponding to the subsonic propeller regime is larger, such that there is only a modest range of (fixed) velocities for which mass loss rate variations in our chosen range ( $0.1 < \dot{M}_{-6} < 100$ ) can cause transitions through all regimes, from the superKeplerian magnetic inhibition to the direct accretion regime. As we discuss below, this has important consequences for the expected luminosity variations.

We now compute the luminosity swings for some of the examples discussed above in a fashion similar to what was done in the context of centrifugally inhibited accretion in NS X-ray transients (Corbet 1996; Campana et al. 1998). Fig. 3A applies to a system with  $\mu_{33}=0.8$ ,  $P_{s3}=1$ , and  $v_8=1.2$  (this corresponds to the case  $P_{s3}=1$  of Fig. 2 panel (a)). The lower panel of this figure shows that, for  $0.1 < \dot{M}_{-6} < 100$ , the magnetospheric radius crosses both the centrifugal ( $R_{co}$ ) and magnetic ( $R_a$ ) barriers. Correspondingly, the system moves from the superKeplerian magnetic inhibition regime, to the supersonic and subsonic propeller regime, and, finally, to the direct accretion regime, giving rise to a six-decade luminosity swing from  $\sim 10^{31}$  to  $\sim 10^{37}$  erg s<sup>-1</sup>. We note that a large part of this swing (about five decades) is attained across the transitions from the superKeplerian magnetic inhibition to the direct accretion regimes, which take a mere factor of  $\sim 5$  variation of  $\dot{M}_w$ .

In the presence of a standard NS magnetic field ( $10^{12}$  G), Fig. 3B shows that such abrupt luminosity jumps are not expected for a very slowly rotating (1000 s) NS (the other system parameters are the same as those of Fig. 3A), since the magnetospheric radius is smaller than both  $R_a$  and  $R_{co}$ , for any reasonable value of  $\dot{M}_w$ . Therefore, the direct accretion regime applies, with the the luminosity proportional to  $\dot{M}_w$ .

<sup>10</sup> This is because, in this region, the mass flow rate is so high that Eq. B2 is violated (the supersonic propeller is no longer self-consistent), and convective motions are damped by radiative cooling.



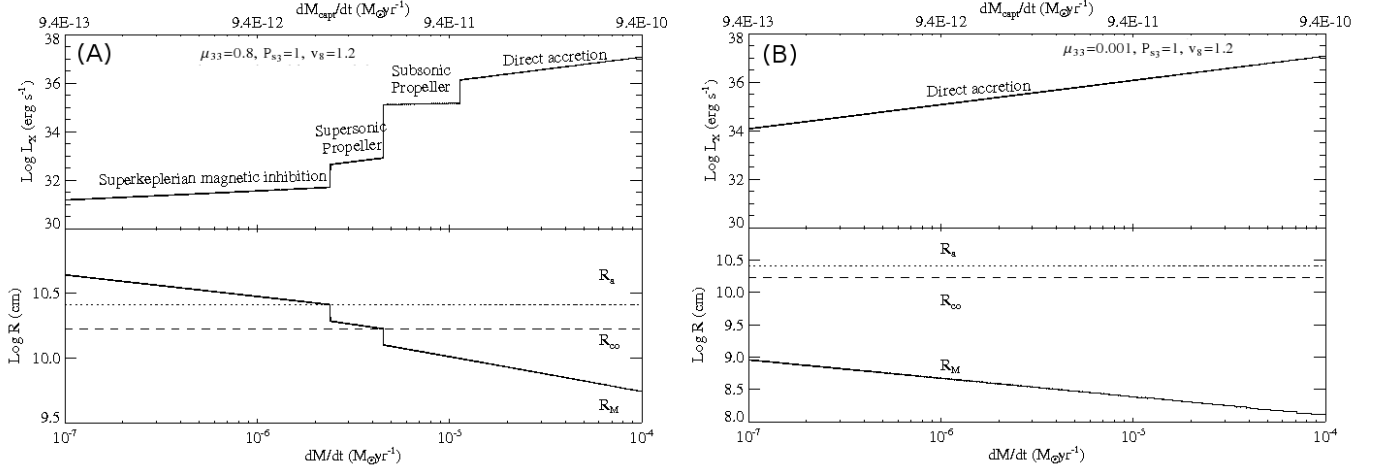


FIG. 3.— (A) *Upper panel*: Variation of the luminosity through different regimes, as a function of the mass loss rate from the companion star. In this case the parameters of the model are fixed at  $\mu_{33}=0.8$ ,  $P_{s3}=1$ , and  $v_8=1.2$ . *Lower panel*: Relative position of the magnetospheric radius,  $R_M$  (solid line), with respect to the accretion radius  $R_a$  (dotted line), and the corotation radius  $R_{\text{co}}$  (dashed line), as a function of the mass loss rate from the companion star. (B) *Upper panel*: Variation of the luminosity through different regimes, as a function of the mass loss rate from the companion star. In this case the parameters of the model are fixed at  $\mu_{33}=0.001$ ,  $P_{s3}=1$ , and  $v_8=1.2$ . *Lower panel*: Relative position of the magnetospheric radius,  $R_M$  (solid line), with respect to the accretion radius  $R_a$  (dotted line), and corotation radius  $R_{\text{co}}$  (dashed line), as a function of the mass loss rate from the companion star.

In Fig. 4 we show the transitions for a system with  $\mu_{33}=0.01$  and  $P_{s3}=0.1$ . The wind velocity is  $v_8=1.2$  in Fig. 4A, and  $v_8=2.2$  in Fig. 4B (see also panel (f) of Fig. 2). These two figures show that, for sub-magnetar fields, a 100 s spinning NS can undergo a transition across the magnetic barrier (besides the centrifugal barrier), for suitable parameters (a high wind velocity in the case at hand). Such transitions take place over a more extended interval of mass loss rates. For instance Fig. 4B shows that an increase by a factor  $\sim 100$  in the mass loss rate is required, in this case, to achieve a factor  $\sim 10^5$  luminosity swing comparable with the magnetar case of Fig. 3A.

In order to illustrate further the role of the magnetic field, spin period and wind velocity, we show in Fig. 5 the way in which the transitions across regimes take place, by holding two of the above variables fixed and stepping the third variable. Figure 5A shows the effect of increasing the value of  $v_8$  from 1 to 1.8 (in turn resulting in a decrease of the accretion radius), in a system with  $\mu_{33}=0.8$  and  $P_{s3}=1$ .

The behaviour of the luminosity changes mainly because a different set of regimes is involved in each case. For  $v_8=1$  (solid line) the system passes through the superKeplerian magnetic inhibition regime, the supersonic, and subsonic propeller regime, finally reaching the direct accretion regime at  $\dot{M}_{-6} \simeq 6$ . In the case  $v_8=1.2$  (dotted line), the transition to the supersonic propeller shifts towards higher mass loss rates, such that superKeplerian magnetic inhibition applies up to  $\dot{M}_{-6} < 2$ . Further increasing the wind velocity to  $v_8=1.4$  (dashed line), the system first undergoes a transition to the subsonic propeller at  $\dot{M}_{-6} \simeq 10$ , bypassing the supersonic propeller (this is because for  $\dot{M}_{-6} \simeq 10$  the magnetospheric radius defined by Eq. 14 is smaller than the corotation radius). As the mass loss rate increases further, the direct accretion regime sets in for  $\dot{M}_{-6} \simeq 20$ . In the case  $v_8=1.8$  (dot-dashed line), the corotation radius exceeds the accretion radius. The system is thus in the superKeplerian magnetic inhibition regime for  $\dot{M}_{-6} < 20$ , while for higher mass loss rates the subKeplerian magnetic inhibition regime applies and the luminosity is dominated by accretion through the KHI. A transition to the direct accretion regime is expected for mass loss rates  $\dot{M}_{-6} > 100$ .

Figure 5B shows the transitions across different regimes for selected values of the magnetic field, in a system with  $P_{s3}=1$  and  $v_8=1.2$ . For the lowest magnetic field in this figure ( $\mu_{33}=0.01$ , solid line), the magnetospheric radius is smaller than both the accretion and corotation radius for the whole range of mass loss rates spanned in the figure, and the system is always in the direct accretion regime. In the case  $\mu_{33}=0.1$  (dotted line), the system is in the subsonic propeller for  $\dot{M}_{-6} < 1$ , while for higher mass inflow rates the direct accretion regime applies. For  $\mu_{33}=0.5$  (dashed line) the luminosity behaviour becomes more complex, as the system goes through the superKeplerian magnetic inhibition regime, the supersonic and subsonic propeller regime, and eventually reaches the direct accretion regime at  $\dot{M}_{-6} \simeq 8$ . For  $\mu_{33}=0.8$  the same sequence of transitions applies, with the entire luminosity swing taking place over a smaller interval of mass loss rates.

Finally, in Fig. 5C we show the effects of increasing the spin period in a system with  $\mu_{33}=0.1$  and  $v_8=1.2$ . For the lowest spin period considered here ( $P_{s3}=0.01$ , solid line), the system remains in the supersonic propeller regime for the whole range spanned by  $\dot{M}_{-6}$ . In the case  $P_{s3}=0.5$  (dotted line) transitions occur from the supersonic propeller regime ( $\dot{M}_{-6} < 0.7$ ), to the subsonic propeller ( $0.7 < \dot{M}_{-6} < 4$ ) and then to the direct accretion regime ( $\dot{M}_{-6} > 4$ ). By

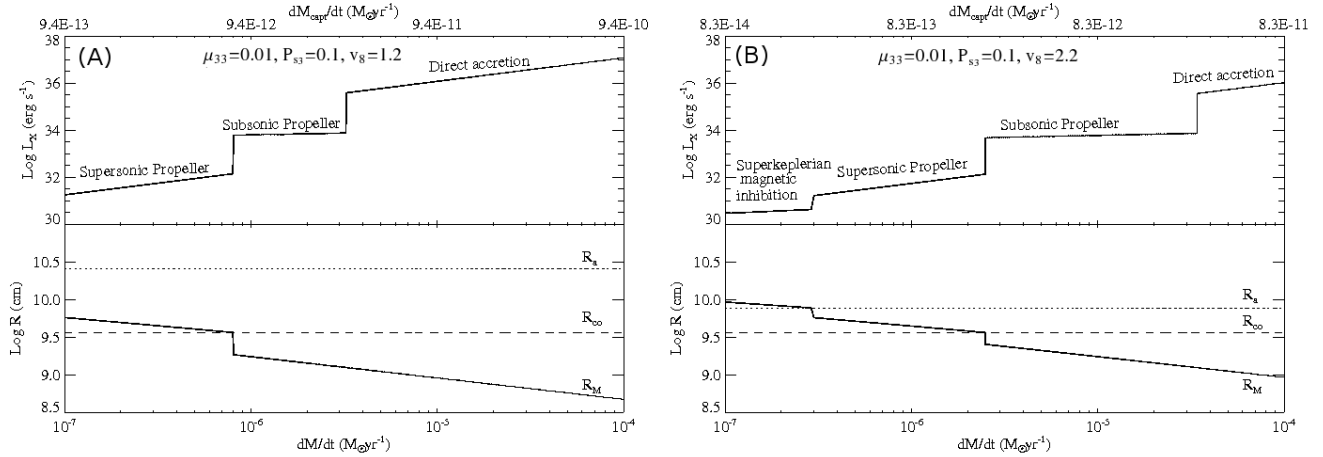


FIG. 4.— (A) *Upper panel*: Variation of the luminosity through different regimes, as a function of the mass loss rate. In this case the parameters of the model are fixed at  $\mu_{33}=0.01$ ,  $P_{s3}=0.1$ , and  $v_8=1.2$ . *Lower panel*: Relative position of the magnetospheric radius,  $R_M$  (solid line), with respect to the accretion radius  $R_a$  (dotted line), and corotation radius  $R_{co}$  (dashed line), as a function of the mass loss rate from the companion star. (B) Same as (A) but for  $\mu_{33}=0.01$ ,  $P_{s3}=0.1$ , and  $v_8=2.2$ .

further increasing  $P_{s3}$  to a value of 1 (dashed line), the system goes through the subsonic propeller and the direct accretion regime, while the supersonic propeller regime does not occur due to the longer spin period as compared to the previous case. For  $P_{s3}=6$  (dot-dashed line) the spin period is so high that the direct accretion regime applies for any reasonable value of  $\dot{M}_{-6}$ .

The above results show that over a range of values of the key parameters  $\mu_{33}$ ,  $P_{s3}$ , and  $v_8$ , large luminosity swings can be achieved with comparatively modest changes in the mass loss rate, as the neutron star undergoes transitions from one regime to another. More generally, these transitions result from changes in the relative position of the accretion, magnetospheric, and corotation radii, reflecting short term variations of the wind velocity and mass loss rate, the only parameters that can vary on shorter timescales than secular. Therefore, transitions between different regimes take place once the source parameters are such that the NS straddles the centrifugal barrier (i.e.  $R_M \simeq R_{co}$ , when  $R_a > R_{co}$ ) or the magnetic barrier (i.e.  $R_M \simeq R_a$ , when  $R_a < R_{co}$ ) or both (i.e.  $R_M \simeq R_{co} \simeq R_a$ ). The centrifugal barrier applies to relatively short spin periods. It is well known that the longer the spin period of a transient neutron star, the higher its magnetic field must be for the centrifugal barrier to operate (see Eqs. 26 and 27). In particular, for periods of hundreds seconds, or longer, magnetic field strengths of  $\gtrsim 10^{13}$ - $10^{14}$  G are required<sup>11</sup>. On the other hand, we have shown that neutron stars with even longer spin periods and magnetar-like fields are expected to undergo transitions across the magnetic barrier and thus are expected to have an inherently different “switch off” mechanism than short spin period systems. A necessary condition for this is that  $R_{co} > R_a$ , which translates into  $P_{s3} \gtrsim 3v_8^{-3}$ . The magnetic and centrifugal barriers set in (nearly) simultaneously (i.e.  $R_a \simeq R_{co} \simeq R_M$ ) for  $\mu_{33} \simeq 0.3P_{s3}^{7/6} \dot{M}_{15}^{1/2}$ .

Taking into account of all the examples discussed in this section, we conclude that:

1. Long spin period systems ( $P_{s3} \gtrsim 1$ ) require magnetar-like B-fields ( $\mu_{33} \gtrsim 0.1$ ) in order for a large luminosity swing ( $\sim 10^5$ ) to arise from modest variations in the wind parameters (e.g. a factor  $\sim 5$  in  $\dot{M}_{-6}$ ). These luminosity swings might result from transition across different regimes through both the centrifugal and magnetic barriers.
2. Shorter spin period systems ( $P_{s3} \ll 1$ ) must possess lower magnetic fields ( $\mu_{33} \ll 0.1$ ) for similar transitions to take place. Somewhat larger variations in the wind parameters are required in order to achieve similar luminosity swings to those of the long period case, and transitions between different regimes occur in most cases through the centrifugal barrier.
3. Few or no transitions are expected for systems with either high magnetic fields and short spin periods, or systems with lower magnetic fields and long spin periods. In the first case the centrifugal barrier halts the inflowing matter at  $R_M$  and accretion does not take place; such systems might thus be observable only at very low (X-ray) luminosity levels ( $\simeq 10^{32}$ - $10^{33}$  erg s<sup>-1</sup>). In the second case  $R_M < R_{co}$  for a wide range of wind parameters, accretion can take place, and a high persistent luminosity is released ( $\simeq 10^{35}$ - $10^{37}$  erg s<sup>-1</sup>).

## 5. APPLICATION TO SFXT SOURCES

In this section we propose that transitions across different regimes caused by relatively mild variations of the wind parameters are responsible for the outbursts of SFXTs. In consideration of the wide range of spin periods inferred for

<sup>11</sup> This point was already noted in Stella et al. (1986).

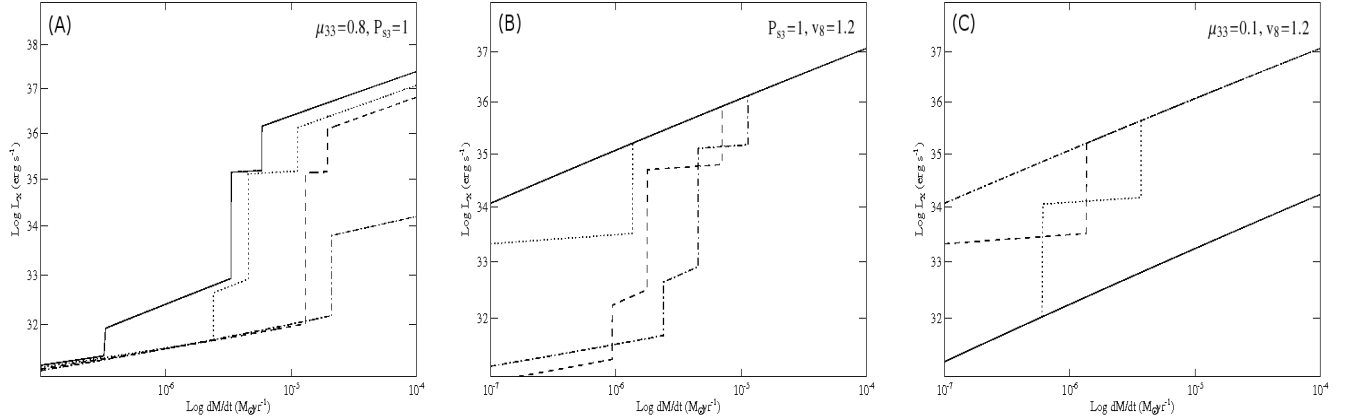


FIG. 5.— Variations of the luminosity through different regimes, as a function of the mass loss rate, for different sets of parameters. (A): In this case we fixed  $\mu_{33}=0.8$  and  $P_{s3}=1$ . The solid line shows luminosity variations for  $v_8=1$ , the dotted line is for  $v_8=1.2$ , and the cases  $v_8=1.4$  and  $v_8=1.8$  are represented with a dashed and dot-dashed line, respectively. (B): Here the fixed parameters are  $P_{s3}=1$  and  $v_8=1.2$ . The different curves correspond to  $\mu_{33}=0.01$  (solid line), 0.1 (dotted line), 0.5 (dashed line), and 0.8 (dot-dashed line). (C): In this case we fixed  $\mu_{33}=0.1$  and  $v_8=1.2$ . Luminosity variations across different regimes are shown for  $P_{s3}=0.01$  (solid line), 0.5 (dotted line), 1 (dashed line), and 6 (dot-dashed line).

SFXTs, the outbursts of these sources are expected to result from the opening of the magnetic barrier in very long spin period systems and the centrifugal barrier in all other systems (see also Grebenev & Sunyaev 2007; Sidoli et al. 2007). More crucially, we conclude that slowly spinning SFXTs should host magnetars, independent of which of the two mechanisms is responsible for their outbursts.

As a case study we consider IGR J17544-2619 (Sunyaev et al. 2003), a SFXT observed by *Chandra* during a complex transition to and from a  $\sim 1$  hour-long outburst, yielding the first detailed characterization of a SFXT light curve. The spin period of IGR J17544-2619 is presently unknown. In’t Zand (2005) showed that four different stages, with very different luminosity levels, could be singled out during the *Chandra* observation: (a) a quiescent state with  $L_X \simeq 2 \times 10^{32}$  erg s $^{-1}$ , (b) a rise stage with  $L_X \simeq 1.5 \times 10^{34}$  erg s $^{-1}$ , (c) the outburst peak with  $L_X \simeq 4 \times 10^{37}$  erg s $^{-1}$ , and (d) a post-outburst stage (or “tail”) with  $L_X \simeq 2 \times 10^{36}$  erg s $^{-1}$  (see panel (a) of Fig. 6; these luminosities are for a source distance of  $\sim 3.6$  kpc, Rahoui et al. 2008). The maximum luminosity swing observed across these stages was a factor of  $\gtrsim 6.5 \times 10^4$ .

Motivated by the evidence for  $>1000$  s periodicities in XTE J1739-302 and IGR J16479-4514 (see § 2), we discuss first the possibility that IGR J17544-2619 contains a very slowly spinning neutron star. We use  $\mu_{33}=1$ ,  $P_{s3}=1.3$ ,  $v_8=1.4$ , and show in Fig. 6(b) the different regimes experienced by such a neutron star as a function of the mass loss rate. For  $\dot{M}_{-6} < 20$  the above values give  $R_M > R_a$  and  $R_M > R_{co}$ , such that superKeplerian magnetic inhibition of accretion applies. The expected luminosity in this regime,  $\sim 10^{31}$  erg s $^{-1}$ , is likely outshined by the X-ray luminosity of the supergiant star (the companion star’s luminosity is not shown in Fig. 6, but it is typically of order  $\sim 10^{32}$  erg s $^{-1}$ , Cassinelli et al. 1981; Berghoefer et al. 2001). We conclude that the lowest emission state (quiescence) of IGR J17544-2619 can be explained in this way, with the companion star dominating the high energy luminosity (In’t Zand 2005). The rise stage is in good agreement with the subKeplerian magnetic inhibition regime, where the luminosity ( $\sim 10^{34}$  erg s $^{-1}$ ) is dominated by accretion of matter onto the NS due to the KHI. The uncertainty in the value of  $h$  translates into an upper limit on the luminosity in this regime which is a factor of  $\sim 10$  higher than that given above (see § 3 and Appendix A).

During the outburst peak the direct accretion regime must apply at a mass loss rate of  $\dot{M}_{-6}=500$ . In this interpretation direct accretion must also be at work in the outburst tail at  $\dot{M}_{-6} \sim 3$ , where a slight decrease in  $\dot{M}_w$  would cause the magnetic barrier to close and the source to return to quiescence. According to this interpretation, if IGR J17544-2619 has a spin period of  $>1000$  s, then it must host a magnetar.

Panel (c) of Fig. 6 shows an alternative interpretation of the IGR J17544-2619 light curve, where we fixed  $\mu_{33}=0.08$ ,  $P_{s3}=0.4$ , and  $v_8=1$ . For this somewhat faster spin (and lower magnetic field), the luminosity variation is mainly driven by a transition across the centrifugal barrier (as opposed to the magnetic barrier). In this case, the quiescent state corresponds to the supersonic propeller regime ( $\dot{M}_{-6} < 0.6$ ), the rise stage to the subsonic propeller ( $0.6 < \dot{M}_{-6} < 2$ ), while both the peak of the outburst and the tail take place in the direct accretion regime at  $\dot{M}_{-6}=200$  and  $\dot{M}_{-6}=10$ , respectively.

Assuming an even faster NS spin period for IGR J17544-2619, a weaker magnetic field would be required. In panel (d) of Fig. 6, we show the results obtained by adopting  $\mu_{33}=0.001$ ,  $P_{s3}=0.01$ , and  $v_8=2$ . The  $\sim 10^{34}$  erg s $^{-1}$  luminosity in the subsonic propeller regime compares well with the luminosity in the rise stage. However, the luminosity of

the supersonic propeller regime is now significantly higher than the quiescence luminosity of  $\sim 10^{32}$  erg s $^{-1}$  (this is consequence of the higher value of  $\dot{M}_w$  for which the supersonic propeller regime is attained in this interpretation). We note that, the whole luminosity swing takes place for a wider range of mass loss rates, and the outburst peak luminosity requires  $\dot{M}_{-6} \simeq 3000$ , an extremely high values even for an OB supergiant.

Interpreting the properties of IGR J17544-2619 in terms of a NS with a spin periods  $\ll 100$  s is more difficult. For instance, for the subsonic propeller regime to set in, the mass loss rate corresponding to the transition across  $R_M = R_{co}$  must be lower than the limit fixed by Eq. 23. If instead the transition takes place at higher mass loss rate, the system goes directly from the supersonic propeller to the direct accretion regime (or vice versa), bypassing the subsonic propeller: therefore, the rise stage would remain unexplained. Since fast rotating NSs require lower magnetic fields for direct accretion to take place while in outburst, Eq. 23 is satisfied only for very high wind velocities ( $v_8 > 2-3$ ). On the other hand, an increase by a factor of  $\sim 2$  in the wind velocity (with respect to the longer spin period solutions) would give a substantially lower  $\dot{M}_{capt}$ , such that the subsonic and the direct accretion regime luminosities fall shortwards of the observed values (unless unrealistically high mass loss rate are considered).

Based on the above discussion, we conclude that IGR J17544-2619 likely hosts a slowly rotating NS, with spin period  $> 100$  s. Whether the magnetic barrier or the centrifugal barrier sets in, causing inhibition of accretion away from the outbursts, will depend on whether the spin period is longer or shorter than  $\sim 1000$  s. We note that IGR J16418-4532, a  $\sim 1240$  s pulsating source with a 3.7d orbital period, displayed short duration flares similar to those of SFXTs and thus might be considered a candidate for hosting an accreting neutron star with a magnetar-like field. However there is no clear evidence yet that IGR J16418-4532 is a transient source, since the very low state revealed with *SWIFT* might well be due to an eclipse (Tomsick et al. 2004; Walter et al. 2006; Corbet et al. 2006).

As another example we discuss the case of IGR J16465-4507, a SFXTs with a spin period of 228 s. The luminosity behaviour of this source is still poorly known. An outburst at  $5 \times 10^{36}$  erg s $^{-1}$  was observed with *INTEGRAL* (assuming a distance of 12.5 kpc, Lutovinov et al. 2005; Smith 2004), which did not detect the source before the outburst down to a level of  $5 \times 10^{35}$  erg s $^{-1}$ . About a week later, *XMM-Newton* revealed the source at  $5 \times 10^{34}$  erg s $^{-1}$  and discovered the 228 s pulsations (Lutovinov et al. 2005; Zurita Heras & Walter 2004). If the direct accretion regime applied all the way to the lowest luminosity level observed so far, then an upper limit of  $\mu_{33} = 0.004$  would be obtained by imposing that the neutron star did not enter the subsonic propeller regime (see Eq. 28). On the other hand, if the luminosity measured by *XMM-Newton* signalled that the source entered the subsonic propeller regime, while direct accretion occurred only during the outburst detected by *INTEGRAL*, then a considerably higher magnetic field of  $\mu_{33} = 0.07$  would be required.

The above discussion emphasizes the importance of determining, through extended high sensitivity observations, the luminosity at which transitions between different source states occur, in particular the lowest luminosity level for which direct accretion is still at work. In combination with the neutron star spin, this can be used to infer the neutron star magnetic field. Alternatively accretion might take place unimpeded at all luminosity levels of SFXTs, a possibility which requires a very clumpy wind as envisaged in other scenarios (Negueruela et al. 2008; Zurita Heras et al. 2007). In this case the neutron star magnetic field can be considerably lower than discussed here. More extensive studies of these sources (and, by analogy, other SFXTs) are clearly required.

## 6. DISCUSSION

If the centrifugal barrier operates in IGR J17544-2619, then the activity of this source (and by extension that of SFXTs with similar properties) should parallel that of long spin period X-ray pulsar transients with Be star companions (Stella et al. 1986). One crucial difference between the two classes, namely the duration of the outbursts, might well result from the presence in Be systems of an accretion disk mediating the flow of matter outside the NS magnetosphere. In fact, while in Be systems the star's slow equatorial wind has enough angular momentum to form such a disk, the supergiant's wind in SFXTs is fast and possesses only little angular momentum relative to the NS. In the absence of a disk, variations in the wind parameters take effect on dynamical timescales, whereas in the presence of a disk they are smoothed out over viscous timescales.

If the spin period is sufficiently long in IGR J17544-2619 and other SFXTs, the onset of the magnetic barrier will inhibit accretion. While steady magnetic inhibition of accretion is familiar, e.g. from the earth magnetosphere - solar wind interaction, transitions in and out of this regime have not yet been observed, to the best of our knowledge. Therefore, very long spin period SFXTs might provide the first opportunity to study transitions across such a magnetic barrier. Irrespective of whether the centrifugal or magnetic barrier operates in IGR J17544-2619, a long spin period would imply a high magnetic field, comparable to those inferred for magnetar candidates.

Scenarios involving magnetars with spin periods well above 1000 s have been considered in several studies (Rutledge 2001; Mori & Ruderman 2003; Toropina et al. 2001; Liu & Yan 2006; Zhang et al. 2004). Moreover a few known accreting X-ray pulsars with unusually long spin periods have already been proposed as magnetar candidates (see e.g., Ikhshanov 2007, and references therein). However these sources display different properties from SFXTs: some are persistent sources; others display week to month-long outbursts; the high spin up measured in IGR J16358-4726 testifies that the accretion flow is likely mediated by a disk (Patel et al. 2007). Therefore some of the features of the model discussed in this paper would not be applicable to these sources.

In the context of wind-fed HMXBs, Zhang et al. (2004) pointed out that magnetars might be hosted in binary systems with relatively short orbits ( $\sim 1-100$  d) and long pulse period ( $\gtrsim 10^3-10^5$  s). By using evolutionary calculations, these authors showed that magnetars would be easily spun-down to such long spin periods by the interaction with the wind

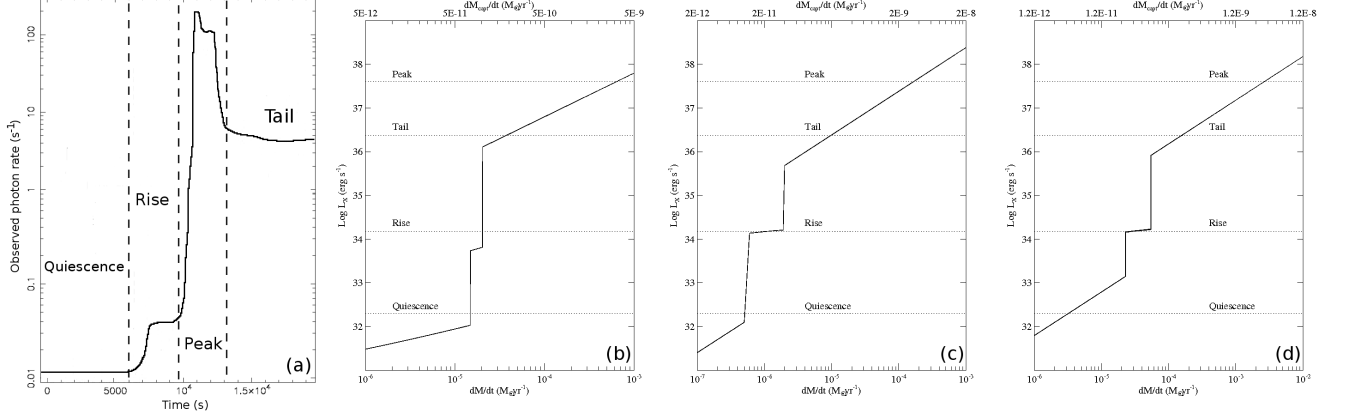


FIG. 6.— Application of the model described in § 3 to the IGR J17544-2619 transition from quiescence to outburst. *Panel (a)*: A schematic representation of the *Chandra* light curve of IGR J17544-2619 obtained by using the segments that were not affected by pile-up (see both panels of figure 2 in In’t Zand 2005). The different luminosity stages are clearly visible. According to In’t Zand (2005), the count rates on the y-axis correspond to  $2 \times 10^{32}$  erg s $^{-1}$ ,  $1.5 \times 10^{34}$  erg s $^{-1}$ ,  $2 \times 10^{36}$  erg s $^{-1}$ , and  $4 \times 10^{37}$  erg s $^{-1}$ , in the quiescence state, the rise state, the tail, and the peak of the outburst, respectively. *Panel (b)*: Interpretation of the quiescence to outburst transition of IGR J17544-2619 in terms of the magnetic barrier model. The dotted horizontal lines mark the luminosity that divide the different regimes. The parameters of the model are fixed at  $P_{s3}=1.3$ ,  $v_8=1.4$ , and  $\mu_{33}=1$ . *Panel (c)*: Interpretation of the quiescence to outburst transition of IGR J17544-2619 based on the centrifugal barrier model. The parameters of the model are fixed at  $\mu_{33}=0.08$ ,  $P_{s3}=0.4$ , and  $v_8=1$ . *Panel (d)*: Same as panel (c) but here the parameters of the model are fixed at  $\mu_{33}=0.001$ ,  $P_{s3}=0.01$ , and  $v_8=2$ .

of the companion star, in less than  $10^6$  yr. The systems we considered in this paper would likely result from a similar evolutionary path.

Once a system approaches the spin period that is required for direct accretion to occur, the short timescale ( $\sim$  hours) erratic variations that characterize a supergiant’s wind will cause transitions across different NS regimes. Insofar as the average wind properties evolve only secularly, the NS spin will then remain locked around such period, alternating spin-up intervals during accretion and spin-down intervals during quiescence, when accretion is inhibited.

The relevant spin-up timescale during accretion intervals is approximately (see e.g. Frank et al. 2002)

$$\tau_{su} = -P_{\text{spin}}/\dot{P}_{\text{spin}} = \Omega I / (\dot{M}_{\text{capt}} l) \simeq 8 \times 10^2 I_{45} v_8^4 P_{10d} P_{s3}^{-1} \dot{M}_{17}^{-1} \text{ yr}, \quad (29)$$

where  $l=2\pi R_a^2/(4P_{\text{orb}})$  the specific angular momentum of wind matter at the accretion radius,  $I=10^{45} I_{45}$  g cm $^2$  the NS moment of inertia, and  $\dot{M}_{17}=\dot{M}_{\text{capt}}/10^{17}$  g s $^{-1}$  (this corresponds to an outburst luminosity of  $\sim 10^{37}$  erg s $^{-1}$ ).

A rough estimate of the spin-down timescale is obtained by assuming that most of the quiescence luminosity draws from the rotational energy of the NS (Davies & Pringle 1981); this gives

$$\tau_{sd} = P_{\text{spin}}/\dot{P}_{\text{spin}} = I\Omega^2/L_X = 1.3 \times 10^2 I_{45} L_{31}^{-1} P_{s3}^{-2} \text{ yr}, \quad (30)$$

where  $L_{31}$  is the luminosity produced by the interaction between the magnetosphere and the wind in units of  $10^{31}$  erg s $^{-1}$ . It is apparent that, for magnetar-like fields and long spin periods the above timescales are much shorter than the lifetime of the supergiant’s strong wind phase. Therefore secular changes in the wind parameters and/or the NS magnetic field will be easily tracked by the NS spin. Moreover since spin-up and spin-down take place on comparable timescales, it is to be expected that spin-up intervals during outbursts are compensated for by spin-down during quiescent intervals of comparable duration. In other words accretion state of long spin period SFXTs would be expected to have a duty cycle of order  $\sim 0.5$  or higher. As we discussed in § 2, evidence for high values of the duty cycle is gradually emerging from high sensitivity observations of SFXTs.

On the other hand spin-down may also occur during the accretion intervals as a results of velocity and density gradients in the supergiant’s wind that lead to temporary reversals of the angular momentum of the captured wind relative to the neutron star (note that persistent wind accreting X-ray pulsars in HMXBs have long been known to alternate spin-up and spin-down intervals, see e.g. Henrichs 1998). This would tend to favor spin-down, such that the NS spin might gradually evolve longwards of the spin period that is required to inhibit direct accretion and a transient source becomes a persistent one. Interestingly, this might apply to 2S 0114+65, a persistent X-ray pulsar with a luminosity of  $\sim 10^{36}$  erg s $^{-1}$ , which displayed variations by a factor of  $\lesssim 10$ . Since its spin period is extremely long ( $\sim 10^4$ )  $R_M$  is smaller than the corotation radius and the NS accretes continuously from the relatively weak supergiant companion’s wind (see also Li & van den Heuvel 1999).

The SFXTs population might thus represent those supergiant HMXBs systems that have not (yet) evolved away from the spin period at which transitions across different NS state can take place.

We note that for SFXTs to host magnetars their dipole magnetic field must retain values in the  $\mu_{33}=0.1-1$  range for a few  $10^6$  yr, i.e. the typical timescale from the formation of the NS to the onset of the supergiant's strong wind. Presently known magnetar candidates (soft gamma repeaters, SGR, and anomalous X-ray pulsars, AXP) have estimated ages in the  $10^4-10^5$  yr range (for a review see e.g. Woods & Thompson 2006). Little is known on the long term evolution of the magnetic field of magnetars and different models have been proposed which lead to different predictions. We note that if the irrotational mode of ambipolar diffusion dominates the B-field decay,  $\mu_{33}=0.1-0.3$  can be expected for ages of a few  $10^6$  yr (Heyl & Kulkarni 1998).

According to our proposed scenario the combination of a long spin period and a very large luminosity swing is indicative of the presence of a magnetar. This can be further corroborated through other magnetars signatures, such as e.g. proton cyclotron features in the X-ray spectrum (Zane et al. 2001) or sporadic subsecond bursting activity such as that observed in AXPs and SGRs (Gavriil et al. 2002).

Finally we remark on the orbital period of SFXTs: in all regimes described in § 3, the luminosity scales with  $L_X \propto P_{\text{orb}}^{-4/3} v_w^{-4}$ . For our fiducial wind parameters, orbital periods of tens of days are required for the transition between low and high luminosity states to occur at  $\simeq 10^{36}$  erg s $^{-1}$ , a typical luminosity for the onset of SFXT outbursts (Walter & Zurita Heras 2007). This is why throughout this paper we scaled our equations by  $P_{\text{orb}}=10$  d and used the same value in the examples of Figs. 2-6. Negueruela et al. (2008) showed that orbital periods around  $\sim 10$  d are compatible with the NSs being embedded in the clumpy wind from the supergiant companions, rather than in a quasi-continuous wind. In this case SFXT outburst durations might be associated with the transit time of a clump

$$\tau_{\text{out}} \simeq a/v_w = 4.2 \times 10^4 a_{10\text{d}} v_8^{-1} \text{ s}, \quad (31)$$

in reasonable agreement with the observed durations of individual flares (see § 2).

We conclude that clumpiness of the stellar wind, an often-used concept for interpreting SFXT activity, applies to the gating scenarios described here as well. The main advantage of introducing a gating mechanism rests with the possibility to model the very large luminosity swings of SFXTs with much milder density (or velocity) contrasts in the wind.

## 7. CONCLUSIONS

In this paper we reviewed the theory of wind accretion in HMXBs hosting a magnetic neutron star with a supergiant companion, and considered in some detail the interaction processes between the inflowing plasma and the magnetosphere that are expected to take place when direct accretion onto the neutron star surface is inhibited. We then applied this theory to SFXTs and showed that their large luminosity swings between quiescence and outburst (up to a factor of  $\sim 10^5$ ) can be attained in response to relatively modest variations of the wind parameters, provided the system undergoes transitions across different regimes. Expanding on earlier work, we found that such transitions can be driven mainly by either: (a) a centrifugal barrier mechanism, which halts direct accretion when the neutron star rotation becomes superKeplerian at the magnetospheric radius, a mechanism that has been discussed extensively in Be star X-ray transient pulsars, or (b) a magnetic barrier mechanism, when the magnetosphere extends beyond the accretion radius. Which mechanism and wind interaction regime apply will depend sensitively on the NS spin period and magnetic field, besides the velocity and mass loss rate in the supergiant's wind. In particular, the magnetic barrier mechanism requires long spin periods ( $\gtrsim 1000$  s) coupled with magnetar-like fields ( $\gtrsim 10^{14}$  G). On the other hand, magnetar-like fields would also be required if the centrifugal barrier set in at relatively high luminosities ( $\gtrsim 10^{36}$  erg s $^{-1}$ ) in neutron stars with spin periods of hundreds seconds.

Evidence has been found that the spin periods of a few SFXTs might be as long as 1000-2000 s. Motivated by this, we presented an interpretation of the activity of IGR J17544-2619 (whose spin period is unknown) in terms of the magnetic barrier by a 1300 s spinning neutron star and showed that the luminosity stages singled out in a *Chandra* observation of this source are well matched by the different regimes of wind-magnetosphere interaction expected in this case. We discussed also an interpretation of this source based on the centrifugal barrier and a slightly shorter spin period (400 s), which reproduced the luminosity stages comparably well. We emphasise that in both solutions the required magnetic field strength ( $\gtrsim 10^{15}$  G and  $\gtrsim 8 \times 10^{13}$  G, respectively) are in the magnetar range.

While the possibility that magnetars are hosted in binary system with supergiant companions has been investigated by several authors (e.g., Zhang et al. 2004; Liu & Yan 2006), clear observational evidence for such extremely high magnetic field neutron star in binary systems is still missing. According to the present study, long spin period SFXTs might provide a new perspective for detecting and studying magnetars in binary systems.

EB thanks the CEA Saclay, DSM/DAPNIA/Service d'Astrophysique for hospitality during part of this work. MF acknowledges the French Space Agency (CNES) for financial support. We would like to thank the referee for useful comments. This work was partially supported through ASI and MUR grants.

## APPENDIX

### ON THE HEIGHT OF THE KHI UNSTABLE LAYER

In this section we expand on the approximation  $h_t \sim R_M$ , introduced previously in § 3.1.2. As discussed by Burnard et al. (1983), the height  $h_t$  of the layer where matter and magnetic field coexist due to the KHI, is mostly determined by the largest wavelength unstable mode of the KHI itself. These authors suggested that

$$h_t \simeq h_{H_s}, \quad (A1)$$

where  $h$  is a factor of order  $\sim 1$ , and  $H_s = R_M^2 k_b T(R_M)/(GM m_p)$  is the scale height of the magnetosheath (note that  $H_s$  is roughly of the same order as  $R_M \simeq 10^{10}$  cm for  $T \sim 10^8$  K). In the subsonic propeller regime, Eq. A1 might be a reasonable assumption due to the presence of an extended atmosphere around the magnetospheric boundary; on the contrary, it cannot be used in the subKeplerian magnetic inhibition regime, where matter flowing toward the NS is shocked very close to the magnetospheric boundary. Despite all these uncertainties, we show below that the assumption  $h_t = h R_M$ , with  $h \sim 1$ , gives a conservative estimate of the mass accretion rate due to the KHI. Using Eq. 8 and the definition  $v_{\text{conv}} = \eta_{\text{KH}} v_{\text{sh}} (\rho_i/\rho_e)^{1/2} (1 + \rho_i/\rho_e)^{-1}$ , we derive the equations that define the ratio of the densities inside ( $\rho_i$ ) and outside ( $\rho_e$ ) the magnetosphere. These are

$$(\rho_i/\rho_e)^{1/2} (1 + \rho_i/\rho_e) = 0.3 \eta_{\text{KH}} h^{-1} R_{\text{M}10}^{3/2} P_{\text{s}3}^{-1}, \quad (\text{A2})$$

if  $v_{\text{sh}} = v_{\text{rot}}$ , and

$$(\rho_i/\rho_e)^{1/2} (1 + \rho_i/\rho_e) = 0.1 \eta_{\text{KH}} h^{-1} R_{\text{M}10}^{1/2} v_8, \quad (\text{A3})$$

if  $v_{\text{sh}} = v_{\text{ps}}$ . Equations A2 and A3 show that  $\rho_i/\rho_e$  is an increasing function of  $h^{-1}$  (for fixed values of  $v_8$ ,  $P_{\text{s}3}$  and  $R_{\text{M}10}$ ). Therefore, being  $v_{\text{conv}} \propto (\rho_i/\rho_e)^{1/2} (1 + \rho_i/\rho_e)^{-1}$  and  $\dot{M}_{\text{KH}} \propto v_{\text{conv}}$ , the KHI rate of plasma entry inside the magnetosphere is also an increasing function of  $h^{-1}$  (provided that  $\rho_i \lesssim \rho_e$ ). Since the KHI unstable layer is located inside the NS magnetosphere, the maximum height attainable is  $h_t = R_M$ , and thus the approximation used in § 3.1.2 and § 3.2.2 gives a lower limit on the mass flow rate controlled by the KHI in both the subKeplerian magnetic inhibition and the subsonic propeller regime.

Note also that the above lower limit does not violate the stability condition of the quasi-static atmosphere in the subsonic propeller regime. In fact, following Ikhsanov (2001c), this atmosphere can be considered quasi-static if the relaxation time scale of the envelope is less than the drift time scale of the mass flow crossing the magnetospheric boundary. In our case matter penetration inside the NS magnetosphere in the subsonic propeller regime is mostly provided by the KHI, and the above condition translates into  $\dot{M}_{\text{KH}} \lesssim (R_M/R_{\text{co}})^{3/2} \dot{M}_{\text{capt}}$ , which is satisfied for a wide range of parameters (see Figs. 3, 4, and 5).

An upper limit to the KHI mass flow rate can be obtained by assuming  $\rho_i/\rho_e = 1$  (a solution adopted, for example, by Rutledge 2001). According to Burnard et al. (1983), the density  $\rho_i$  can be increased until the thermal pressure inside the magnetosphere  $p_i \propto \rho_i$  is comparable to the magnetic pressure  $p_m = B^2(R_M)/(8\pi)$ . When this limit is reached, an instability occurs on the lower surface of the unstable layer that increases  $h_t$  until  $p_i < p_m$  is restored. Using the post-shocked gas temperature at  $R_M$  (see § 3), it is shown that  $\rho_i/\rho_e \sim 1$  does not violate the condition  $p_i < p_m$  (at least in the subKeplerian magnetic inhibition regime). Therefore, even though we restricted ourself to the lower limit  $h = 1$ , the upper limit on  $\dot{M}_{\text{KH}}$  might be attainable in some instances. The KHI would then provide matter penetration inside the magnetosphere at a rate  $\sim \dot{M}_{\text{capt}}$ , thus allowing almost all the captured matter to accrete onto the NS. A detailed calculation of KHI accretion in the subKeplerian magnetic inhibition and subsonic propeller regimes will be reported elsewhere.

## RADIATIVE LOSSES IN THE SUPERSONIC PROPELLER

As shown by Davies & Pringle (1981), the treatment of the supersonic propeller regime (see § 3.2.1) is self consistent only if the energy input at the base of the atmosphere, due to the supersonic rotating NS magnetosphere, is larger than radiative losses within the atmosphere itself. The range of validity of this assumption can be determined by using the convective efficiency parameter

$$\Gamma = \mathfrak{M}_t^2 v_t(R) t_{\text{br}}(R) R^{-1}, \quad (\text{B1})$$

where  $\mathfrak{M}_t = v_t(R)/c_s(R)$  is the Mach number,  $v_t$  and  $c_s$  are the turbulent and sound velocity, and  $t_{\text{br}} = 2 \times 10^{11} T^{1/2} m_p \rho^{-1}(R)$  s is the bremsstrahlung cooling time. For most of the NS rotational energy dissipated at the magnetospheric radius to be convected away through the atmosphere's outer boundary,  $\Gamma$  should be  $\gtrsim 1$  across the entire envelope. Taking into account that in the supersonic propeller regime  $v_t \simeq c_s$ ,  $c_s \sim v_{\text{ff}}$ ,  $T \sim T_{\text{ff}}$  and  $\rho$  is given by Eq. 13, one finds  $\Gamma \propto R^{-3/2}$ . Therefore the said requirement is satisfied when  $\Gamma(R_a) \gtrsim 1$ , i.e.

$$\dot{M}_{-6} \lesssim 2.2 \times 10^2 v_8^5 a_{10d}^2. \quad (\text{B2})$$

For mass loss rates larger than the above limit, radiative losses are not negligible and the treatment used in § 3.2.1 for the supersonic propeller regime is no longer self-consistent. We checked that the limit of Eq. B2 is never exceeded in the cases of interest. We note that a similar value was also derived by Ikhsanov (2002), but his limit is a factor 10 larger than ours. This might be due to the fact that Ikhsanov (2002) used  $\rho_w$  instead of  $\rho_{\text{ps}}(1+16/3)^{1/2}$  in the expression for the matter density at  $R_a$ .

## RADIATIVE LOSSES IN THE SUBSONIC PROPELLER

A similar calculation to that in Appendix B in the subsonic propeller regime shows that  $\Gamma \propto R^{1/2}$ , and radiative losses are negligible if  $\Gamma(R_M) \gtrsim 1$ , i.e.

$$\dot{M}_{-6} \lesssim 2.8 \times 10^2 P_{\text{s}3}^{-3} a_{10d}^2 v_8 R_{\text{M}10}^{5/2} (1 + 16 R_{a10}/(5 R_{\text{M}10}))^{-3/2}, \quad (\text{C1})$$

that is the same value as that in Eq. 23 (a somewhat different value was obtained by Ikhsanov (2001a) assuming a density  $\simeq \rho_w$  at  $R_M$  instead of  $\rho_{ps}(1+16R_M/(5R_a))^{3/2}$ ).

## REFERENCES

- Bamba, A., Yokogawa, J., Ueno, M., Koyama, K., & Yamauchi, S. 2001, PASJ, 53, 1179
- Berghoefer, T. W., Schmitt, J. H. M. M., Danner, R., & Cassinelli, J. P. 1997, A&A, 322, 167
- Bondi, H. 1952, MNRAS, 112, 195
- Burnard, D. J., Arons, J., & Lea, S. M. 1983, ApJ, 266, 175
- Campana, S., Colpi, M., Mereghetti, S., Stella, L., Tavani, M. 1998, A&ARv, 8, 279
- Cassinelli, J. P., Waldron, W. L., Sanders, W. T., Harnden, F. R., Rosner, R., & Vaiana, G. S. 1981, ApJ, 250, 677
- Corbet, R. H. D. 1996, ApJ, 457, L31
- Corbet, R., et al. 2006, Astr. Tel., 779
- Davidson, K. & Ostriker, J. P. 1979, ApJ, 179, 585
- Davies, R. E., Fabian, A. C., & Pringle, J. E. 1979, MNRAS, 186, 779
- Davies, R. E. & Pringle, J. E. 1981, MNRAS, 196, 209
- Dessart, L. & Owocki, S.P. 2003, A&A, 406, L1
- Duncan, R. C. & Thompson, C. 1992, ApJ, 392, L9
- Elsner, R. F. & Lamb, F. K. 1977, ApJ, 215, 897
- Frank J., King A., & Rayne D. 2002, Accretion Power in Astrophysics (3th ed., Cambridge: Cambridge University Press)
- Gavriil, F. P., Kaspi, V. M., & Woods, P. M. 2002, Nature, 419, 142
- González-Riestra, R., Oosterbroek, T., Kuulkers, E., Orr, A., & Parmar, A. N. 2004, A&A, 420, 589
- Götz, D., Falanga, M., Senziani, F., De Luca, A., Schanne, S., & von Kienlin, A. 2007, ApJ, 655, L101
- Grebenev S. A. & Sunyaev, R. A., 2005, AstL, 31, 672
- Grebenev S. A. & Sunyaev, R. A., 2005, AstL, 33, 149
- Halpern, J. P., Gotthelf, E. V., Helfand, D. J., Gezari, S., & Wegner, G. A. 2004, Astr. Tel., 289
- Harding, A. K. & Leventhal, M. 1992, Nature, 357, 388
- Heyl, J. S. & Kulkarni, S. R. 1998, ApJ, L61
- Henrichs, H. F., 1983, in Accretion-driven stellar X-ray sources, ed. W. H. G. Lewin & E. P. J. van den Heuvel (Cambridge, UK: Cambridge University Press), 393
- Ikhsanov, N. R. & Pustil'nik, L. A. 1996, A&A, 312, 338
- Ikhsanov, N. R. 2001a, A&A, 368, L5
- Ikhsanov, N. R., Larionov, V. M., & Beskrovnaya, N. G. 2001b, A&A, 372, 227
- Ikhsanov, N. R. 2001c, A&A, 375, 944
- Ikhsanov, N. R. 2002, A&A, 381, L61
- Ikhsanov, N. R. 2007, MNRAS, 375, 698
- Illarionov, A. F. & Sunyaev, R. A. 1975, A&A, 39, 185
- In 't Zand 2005, A&A, 441, L1
- Kennea, J. A. & Campana, S. 2006, Astr. Tel., 818
- Leyder, J.-C., Walter, R., Lazos, M., Masetti, N., & Produit, N. 2007, A&A, 465, L35
- Li, X.-D. & van den Heuvel, E.P.J. 1999, ApJ, 513, L45
- Lipunov, V. M. 1992, Astrophysics of Neutron Stars (Springer-Verlag)
- Liu, Q. Z. & Yan, J. Z. 2006, AdSpR, 38, 2906
- Lutovinov, A., Revnitvsev, M., Gilfanov, M., Shtykovskiy, P., Molkov, S., & Sunyaev, R. 2005, A&A, 444, 821
- Masetti, N., et al. 2006, A&A, 449, 1139
- Mori, K. & Ruderman, M. A. 2003, ApJ, 592, L75
- Negueruela, I., Torrejon, J. M., Reig, P., Ribo, M., & Smith, D. M. 2008, preprint (astro-ph/0801.3863)
- Nespoli, E., Fabregat, J., & Mennickent, R. 2007, Astr. Tel., 983
- Patel, S.K., et al. 2007, ApJ, 657, 1003
- Perna, R., Bozzo, E., & Stella, L. 2006, ApJ, 639, 363
- Prinja, R. K., Massa, D., & Searle, S. C. 2005, A&A, 430, L41
- Rahoui, F., Chaty, S., Lagage, P.-O., Pantin, E. 2008, preprint (astro-ph/0802.1770)
- Rutledge, E. R. 2001, ApJ, 553, 796
- Sguera, V., et al. 2005, A&A, 444, 221
- Sguera, V., et al. 2006, ApJ, 646, 452
- Sguera, V., et al. 2007, A&A, 462, 695
- Sidoli, L., Vercellone, S., Mereghetti, S., & Tavani, M. 2005, A&A, 429, L47
- Sidoli, L., Romano, P., Mereghetti, S., Paizis, A., Vercellone, S., Mangano, V., & Gtz, D. 2007, A&A, 476, 1307
- Smith, D. M. 2004, Astr. Tel., 338
- Smith, D. M., Heindl, W. A., Markwardt, C. B., Swank, J. H., Negueruela, I., Harrison, T. E., & Huss, L. 2006, ApJ, 638, 974
- Stella, L., White, N. E., & Rosner, R. 1986, ApJ, 308, 669
- Sunyaev, R. A., Grebenev, S. A., Lutovinov, A. A., Rodriguez, J., Mereghetti, S., Gotz, D., & Courvoisier, T. 2003, Astr. Tel., 190
- Tauris, T. M. & van den Heuvel, E. P. J. 2006, in Formation and evolution of compact stellar X-ray sources, ed. W. Lewin & M. van der Klis (Cambridge, UK: Cambridge University Press), 623
- Tomsick, J. A., Lingenfelter, R., Corbel, S., Goldwurm, A., & Kaaret, P. 2004, Astr. Tel., 224
- Tomsick, J. A., Chaty, S., Rodriguez, J., Foschini, L., Walter, R., & Kaaret, P. 2006, ApJ, 647, 1309
- Toropina, O. D., Romanova, M. M., & Lovelace, R. V. E. 2006, MNRAS, 371, 569
- Toropina, O. D., Romanova, M. M., Toropin, Y. M., & Lovelace, R. V. E. 2001, ApJ, 561, 964
- van den Heuvel, E. P. J. & Rappaport, S. 1987, in Physics of Be stars (Cambridge, UK: Cambridge University Press), 291
- Verbunt, F. & van den Heuvel, E. P. J. 1995, X-ray binaries, ed. W. H. G. Lewin, J. van Paradijs, E. P. J. van den Heuvel, (Cambridge, UK: Cambridge University Press), 457
- Walter, R., et al. 2006, A&A, 453, 133
- Walter, R. & Zurita Heras, J. A. 2007, A&A, 476, 335
- Woods, P. M. & Thompson, C. 2006, in Compact stellar X-ray sources, ed. W. Lewin & M. van der Klis (Cambridge, UK: Cambridge University Press), 547
- Zane, S., Turolla, R., Stella, L., & Treves, A. 2001, ApJ, 560, 384
- Zhang, F., Li, X.-D. & Wang, Z.-R. 2004, ChJAA, 4, 320
- Zurita Heras, J. A. & Walter, R. 2004, Astr. Tel., 336
- Zurita Heras, J. A., Chaty, S., & Rodriguez, J. 2007, Astr. Tel., 1035